Soft Matter

PAPER

View Article Online
View Journal | View Issue

Check for updates

Cite this: *Soft Matter*, 2025, **21**, 6575

Windmill droplets: optically induced rotation of biphasic oil-in-water droplets

Jesús J. del Pozo, †[a] Ana B. Bonhome-Espinosa, †[a] Wei Sun,[ab] Carlos Gutiérrez-Ariza,[a] Raúl A. Rica-Alarcón *[ac] and Laura Rodríguez-Arco *[acd]

Received 14th March 2025,
Accepted 28th July 2025

DOI: 10.1039/d5sm00273g

rsc.li/soft-matter-journal

In the field of microdroplet manipulation, optical tweezers have been used to form and grow droplets, to transport them, or to measure forces between droplet pairs. However, the exploration of out-of-equilibrium phenomena in optically trapped droplets remains largely uncharted. Here, we report the rotation of biphasic droplets fabricated by co-emulsifying two immiscible liquids (*i.e.*, hydrocarbon and fluorocarbon oils) with a refractive index mismatch in water. When trapped, droplets of a specific geometry rotate around the axis of the laser beam, in what appears to be a dissipative, out-of-equilibrium phenomenon. The rotational frequency, obtained from image analysis, is stable and proportional to the beam power. Remarkably, droplets that do not interact with the trapping beam can also be rotated indirectly. This is achieved by positioning the droplets at the center of a circular arrangement of multiple, sequentially activated traps, so that the droplet orients towards the location of the active trap. Altogether, our results demonstrate out-of-equilibrium phenomenology in optically trapped biphasic droplets, which would inspire the development of devices based on them (*e.g.*, optically induced mixing, *etc.*). In addition, they may shed light on fundamental principles of optical manipulation of asymmetric particles.

Open Access Article. Published on 30 Juli 2025. Downloaded on 02.04.2026 06:31:57.
This article is licensed under a Creative Commons Attribution-NonCommercial 3.0 Unported Licence.

Introduction

The manipulation of tiny volumes of liquids in the form of droplets is already revolutionizing fields such as biotechnology, healthcare and materials science. The rapid heat and mass transfer within droplets, combined with reduced reagent consumption and waste production, enhances reaction rates and yields, thereby improving sustainability.[1,2] This is particularly advantageous for high-throughput screening of reaction conditions in genomics or drug discovery, and for conducting rapid, on-site testing of minimal sample sizes in diagnostics (*e.g.*, digital PCR or hyperspectral imaging). Additionally, droplet-based templating can be exploited to fabricate complex hierarchical structures, which could find applications in sensors, actuators, energy storage, biomedical implants, and other smart devices.[1–6]

In the last decade there has been significant progress in remotely manipulating droplets by external forces (*i.e.*, active manipulation), utilizing electric or magnetic fields, acoustic waves, thermal forces or optical manipulation.[5] These techniques enable control over droplet dynamics such as movement and positioning, fusion and mixing, fission, and sorting. In particular, light-driven methods enable high-resolution spatiotemporal control and reconfigurability, thanks to the ease of tuning the intensity, position, shape or pattern of the laser beam. They also eliminate the need of adding electrodes or wiring.[5] Notably, optical tweezers, which utilize a highly focused Gaussian beam to confine, move and rotate particles, stand out in terms of precision, dynamic control, scalability and versatility.[7,8] In microemulsion droplet technology optical tweezers have been used to form and grow microdroplets,[9,10] to move them to specific locations,[9] or to measure the force between pairs of droplets.[11–13] However, the exploration of out-of-equilibrium phenomena in optically trapped emulsion droplets remains almost unexplored, despite the interest from the fundamental and applied viewpoints of these.[14,15]

In general, when particles are placed near the focus of the Gaussian beam in optical tweezers setups, they experience two forces: the gradient force and the scattering force.[16,17] In the case of a dielectric particle whose refractive index (n_p) is larger than that of the surrounding medium (n_m), the light that impinges the particle from the medium bends (refracts) towards the higher refractive index material, leading to a

[a] *Universidad de Granada, Department of Applied Physics, Campus de Fuentenueva S/N, 18071, Granada, Spain. E-mail: rul@ugr.es, l_rodriguezarco@ugr.es*
[b] *Department of Physics, Yanshan University, 066004, Qinhuangdao, China*
[c] *Nanoparticle Trapping Laboratory, Research Unit 'Modeling Nature' (MNat), Universidad de Granada, 18071 Granada, Spain*
[d] *Instituto de Investigación Biosanitaria Ibs, GRANADA 18014, Granada, Spain*
† These authors contributed equally.

Open Access Article. Published on 30 Juli 2025. Downloaded on 02.04.2026 06:31:57.
This article is licensed under a Creative Commons Attribution-NonCommercial 3.0 Unported Licence.

gradient force that pulls the particle towards the regions of highest intensity, at the focus. The scattering force, caused by the radiation pressure from the momentum transfer of the beam photons, always pushes the particle along the direction of the beam's propagation. Therefore, under appropriate conditions, particles with a refractive index higher than that of the surrounding medium ($n_p > n_m$) experience gradient forces that can overcome scattering forces, trapping the particles at a stable position close to the focus of the beam. Conversely, particles with a lower refractive index than the surrounding medium ($n_p < n_m$) cannot be trapped with this configuration, because the gradient force pushes the particle away from the focus when the refractive index contrast is negative ($n_p - n_m < 0$).[18]

Due to the substantial influence of the refractive index in optical trapping experiments, here we were intrigued by the potential outcome of co-emulsifying two immiscible liquids with refractive index mismatch within a single droplet. These biphasic droplets, based on liquid–liquid phase separation, represent a fascinating frontier in droplet technology.[19] The asymmetry intrinsic to these droplets offers unique possibilities in terms of chemical composition and functionalities, enabling each region of the droplet to behave differently in response to external cues. Indeed, asymmetry has been exploited to prompt out-of-equilibrium behaviours, such as droplet self-propulsion.[20,21] Particularly interesting are oil-in-water biphasic droplets, where the inner phase consists of a mixture of a hydrocarbon oil and a fluorocarbon oil. From an optical standpoint these are noteworthy, because the refractive index of the hydrocarbon oil is higher than that of water, while the refractive index of the fluorocarbon oil is lower than the refractive index of water.[22–25] In addition, these droplets undergo dynamic morphological transitions in response to external stimuli. Specifically, they can be reconfigured between double emulsion droplets and Janus droplets.[19] This property has been exploited, for example, to fabricate tuneable compound lenses, which can behave as either diverging or focusing lenses depending on the droplet morphology.[22,23]

Prompted by their fascinating properties, here we prepare oil-in-water biphasic droplets using hydrocarbon (dodecane) and fluorocarbon (2-(trifluoromethyl)-3-ethoxydodecafluorohexane) oil mixtures as the inner phase. At room temperature, the two oils are immiscible leading to the formation of distinct phases within the droplets, which creates an asymmetrical refractive index profile. We investigate their trapping capabilities in a commercial optical tweezers setup to find out that out-of-equilibrium droplet rotation, not reported previously, arises. Rotation is dependent on the droplet morphology and can be accelerated by increasing the laser beam power. In addition, we demonstrate that it is also possible to externally induce user-defined droplet rotation by shining a laser in the vicinity of the droplets (*i.e.*, when the droplets are not trapped). Overall, our results show complex, out-of-equilibrium interactions in an optical trap setting, which might provide insights into fundamental principles of optical manipulation of asymmetric particles.

Methods

Materials

n-Dodecane (99% purity for synthesis, Merck USA, density of 0.750 g cm^{-3}) and 2-(trifluoromethyl)-3-ethoxydodecafluorohexane (HFE-7500 3M™ Novec™ 7500 Engineered Fluid, Fluorochem, United Kingdom, density of 1.614 g cm^{-3}) were used as hydrocarbon (HC) and fluorocarbon (FC) oils, respectively. The anionic hydrocarbon surfactant sodium dodecyl sulfate (SDS, 95% purity, Scharlab, Spain) was used as surfactant for the dodecane phase, while the fluorinated surfactant Capstone® FS-30 (Apollo Scientific, United Kingdom) was chosen as stabiliser for the HFE-7500 phase.

Droplet fabrication

To fabricate the biphasic droplets, we first prepared a stock emulsion by dispersing 100 μL of a 1 : 1 mixture of dodecane and HFE-7500 into 500 μL of an aqueous solution of Capstone (0.007 wt%) and SDS (0.025 wt%). The dispersion was conducted using a homogenizer (IKA Ultra-Turrax T 10 basic, Germany) set at 30 000 rpm for 30 s. To engineer the desired morphology, 5 μL of the stock emulsion was pipetted into 500 μL of a given surfactant solution in water (composition detailed in Table 1 below) to allow for reconfiguration of the droplet. The morphology was left to equilibrate for 24 h before optical trapping experiments.

Monophase control samples of dodecane or HFE-7500 alone were prepared by emulsifying 100 μL of the oil in 500 μL of 0.05 wt% solutions of SDS and 0.014 wt% solutions of Capstone, respectively. For optical tweezers experiments these samples were diluted by pipetting 5 μL of the stock in 500 μL of the same surfactant solutions (see Table 1).

Optical microscopy images of the as-prepared samples (recorded with an Olympus U-TV0.5XC-3 microscope (Achilles, Japan)) are shown in Fig. S1 and S2.

Optical trapping experiments

Optical trapping experiments were conducted in a commercial optical-tweezers setup (NanoTracker-II from JPK-Bruker, Germany) equipped with a 2 W steerable laser (wavelength λ = 1064 nm, linear polarization) focused by a Zeiss objective "C-Apochromat" 63x/1.20, WD 0.28 mm, NA 1.2. The forward scattered light from trapped specimens is directed to a quadrant photodiode (QPD) that provides a voltage signal that is proportional to the motion of trapped particles in the trap, as we discuss below. Observation chambers were fabricated by carefully depositing two fine seams of high viscosity sealing paste (Korasilon paste, Kurt Obermeier GmbH, Germany) on a

Table 1 Composition of the surfactant solution

Sample	Composition
FC-in-HC	0.035 wt% SDS 0.004 wt% Capstone
HC-in-FC	0.014 wt% Capstone
HC control	0.05 wt% SDS
FC control	0.014 wt% Capstone

 This journal is © The Royal Society of Chemistry 2025

Open Access Article. Published on 30 Juli 2025. Downloaded on 02.04.2026 06:31:57.
This article is licensed under a Creative Commons Attribution-NonCommercial 3.0 Unported Licence.

#1.5 glass slide, which was then covered with a smaller #1.5 coverslip. The height of the sample chamber was around 120 μm, that is roughly one-two orders of magnitude larger than the droplet size (in the range 1–20 μm). Around 50 μL of the droplet sample were pipetted in between the two glass layers and the chamber was sealed using the same sealing paste.

In the control oil experiments, we focused on a given monophase droplet and tested whether it could be trapped (*i.e.*, dodecane-based) or not (*i.e.*, HFE-based). Movies were recorded. In the case of the biphasic droplets, trapping and rotation did not automatically occur. To achieve trapping, the focus of the laser beam had to be located at the HC part of the FC-in-HC droplets. Otherwise, the droplet was repelled from the beam. In order to induce rotation, we typically proceeded as follows. Droplets settled at the bottom of the chamber due to their weight. Activating the trap led to the upwards laser beam pushing them into the bulk thanks to the scattering force. We then briefly switched off the trap in order to allow the denser FC part of the droplet to settle below the laser focus. When the HC part was at the height of the focus, the trap was switched on, the droplet was effectively trapped and the droplet typically initiated rotation. We varied the laser power in the range 10–122 mW and recorded videos of the rotation for three different droplets. We also recorded the power spectral density (PSD) of the time traces for a rotating FC-in-HC droplet as a function of frequency (f). We then fitted the experimental data to a Lorentzian curve:[17]

$$\mathrm{PSD}(f) = \frac{D}{2\pi^2(f_c^2 + f^2)} \quad (1)$$

where D is the diffusion coefficient of the trapped particle and $f_c = \kappa/2\pi\gamma$ represents the cutoff frequency, related to the stiffness of the trap κ and the friction coefficient γ.

In addition, we recorded droplet tilt and translation towards the laser beam when the latter was focused on the vicinity of the biphasic (both HC-in-FC and FC-in-HC) droplets (*i.e.*, in the absence of trapping). In this regard, we also focused the beam at specific locations within the droplet vicinity to externally induce rotation. To do this, we arranged twelve traps into a circumference pattern, following the layout of a 12-hour clock. The traps were sequentially activated and the dwell time (*i.e.*, the duration for which the laser remained switched on in a particular trap) was varied from 20 ms to 1 s.

Image analysis

Analysis of the droplet rotational trajectories and calculation of the rotational frequencies were performed using Phyton and the numerical computing/plotting libraries NumPy and Matplotlib. The Imageio library was used to extract metadata from the images.

The script initially applied a frame-by-frame thresholding procedure to create a binary (1-0) image. Thresholding involved a threshold value, and an approximate droplet radius provided by the user. Pixels with intensities above the threshold were set to white (1), while those below were set to black (0). Using this binary image as a starting point, the script then fitted the droplet contour to an ellipse using the user-provided radius value as an initial guess and identified the midpoint between the foci. The script tracked the position of this midpoint and generated a file containing the x, y coordinates over time. Because the droplets stayed roughly elliptical during the rotation motion, the ellipse center (or foci midpoint) worked fine as a reference. If, for some reason, the script failed to detect an ellipse for a particular frame, it prompted the user to provide new threshold and radius values.

The rotational frequencies of x and y were determined by fitting plots of these parameters against time with a sine function for each laser power. Fitting was performed for time intervals of 1, 2, 5, 10, 20 and 30 s (sampling times) to find out that the obtained frequencies did not depend on the sampling time (see Fig. S3). The values plotted in the main text represent the average frequency across all sampling times.

Results

To investigate the optical trapping behaviour of droplets with an asymmetrical refractive index distribution, we prepared biphasic oil-in-water (O-in-W) droplets where the oil phase was a mixture of a hydrocarbon (HC) oil, dodecane (refractive index n_{HC} = 1.421 > n_{water} [1064 nm] = 1.326), and a fluorocarbon (FC) oil, 2-(trifluoromethyl)-3-ethoxydodecafluorohexane (commercially known as HFE-7500 3M™ Novec™ 7500 Engineered Fluid, refractive index n_{FC} = 1.29 < n_{water}). Because these two oils are immiscible at room temperature, they gave rise to phase separation within the droplets, as shown in Fig. 1a–d. As previously reported,[19] we were able to prepare droplets with two thermodynamically permitted configurations depending on the interfacial tensions of the HC–W, the FC–W, and the HC–FC interfaces, denoted as γ_{HC}, γ_{FC}, and γ_{HC-FC}, respectively. To modulate these, we used mixtures of solutions of a fluorinated surfactant (Capstone) and of a hydrocarbon surfactant (SDS) as aqueous phase for droplet formation. When Capstone was in higher proportion (γ_{HC}–$\gamma_{FC} \geq \gamma_{HC-FC}$), the FC oil completely encapsulated the HC oil, forming HC-in-FC droplets (Fig. 1a, b and Fig. S1). Conversely, when SDS predominated (γ_{FC}–$\gamma_{HC} \geq \gamma_{HC-FC}$) the HC oil encapsulated the FC oil, resulting in FC-in-HC droplets (Fig. 1c, d and Fig. S1). Monophase control droplets consisting of either HC oil (in a SDS solution) or FC oil (in a Capstone solution) were also fabricated for comparison (Fig. S2).

We then inspected the samples in the optical tweezers setup (Fig. 1e). We began by analysing the monophase droplets. HC droplets could be easily trapped close to the beam waist of the laser and dragged along with it (see Fig. 2a and Movie S1). We attributed this behaviour to the refractive index mismatch between the dodecane (n_{HC} = 1.421) and water (n_W = 1.326). On the other hand, when FC droplets were placed in the observation chamber optical trapping was not possible. Instead, these droplets were repelled by the laser when the beam was translated across the field of view, resulting in net droplet transport as well (see Fig. 2b and Movie S2). This was consistent with the lower refractive index of the FC oil (n_{FC} = 1.29) compared to that of water.[25]

Open Access Article. Published on 30 Juli 2025. Downloaded on 02.04.2026 06:31:57.
This article is licensed under a Creative Commons Attribution-NonCommercial 3.0 Unported Licence.

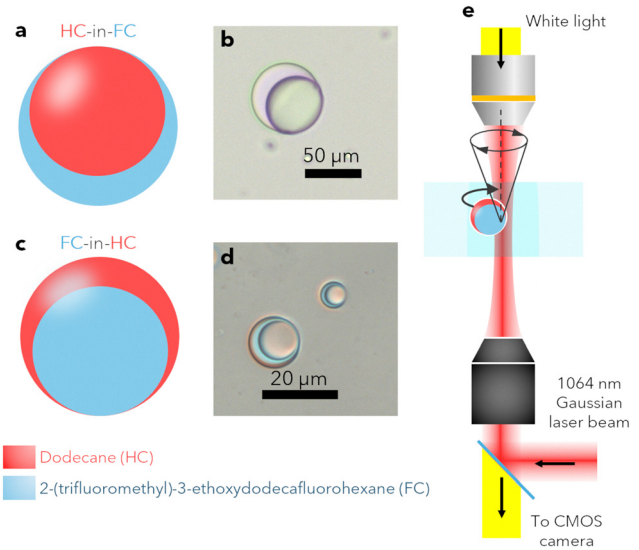

Fig. 1 Schematics (a) and (c) and optical microscopy images (b) and (d) of oil-in-water biphasic droplets with hydrocarbon (HC) and fluorocarbon (FC) oil mixtures as inner phase. Depending on the surfactant composition of the aqueous phase two distinct morphologies could be prepared: droplets in which the FC oil encapsulated the HC oil (HC-in-FC) (a) and (b) or droplets with the FC oil being encapsulated by the HC one (FC-in-HC) (c)–(e). Schematics of the optical tweezers setup. The droplets were trapped close to the focus of a Gaussian laser beam. The droplet was arranged in the trap such that the HC phase was located close to the focus of the beam.

Given the opposite behaviour of the control droplets in their interaction with the laser beam, we wondered how biphasic droplets would behave when placed in the optical tweezers setup. Both HC-in-FC and FC-in-HC droplets could be stably trapped with the beam. Remarkably, under specific conditions (please, see Methods section), FC-in-HC droplets started to rotate around the laser beam axis, with stable rotation frequency (see Fig. 2c and Movie S3). The motion was neither orbital[26] nor spin[8] like. Instead, we observed that the droplet was trapped at a fixed position, apparently close to the interface between the two oils, and the droplet rotated around this point very much as a Bravais pendulum would do around its suspension point.[27] The rotation was well maintained for long periods (several minutes), although the rotation direction often reversed, *i.e.*, switching from counterclockwise to clockwise (Movie S4). Rotation stopped as soon as the laser was switched off, and was accelerated when the power of the beam was increased. On the other hand, HC-in-FC droplets did not show any rotational motion, but enhanced fluctuations which increased with increasing beam power (Movie S5).

We analysed the rotation motion of the FC-in-HC droplets by image analysis using a script in Phyton. Briefly, we fitted the droplet contour with an ellipse, identified the middle point between the foci and tracked the position of this point (*i.e.*, its x, y coordinates). The trajectory plot (y *vs.* x plot) confirmed that the droplet followed a circular path (Fig. 3a). Both the x and y coordinates oscillated with well-defined period and approximately constant amplitude (Fig. 3b and c, respectively). We quantified the rotation frequency by fitting the plots of the temporal evolution of x and y with a sine function for each laser power and confirmed that the frequency was roughly the same for the two parameters (Fig. S3).

As described before, when the laser power was increased from 10 to 122 mW, the rotation speed seemed to increase. We corroborated these observations by image analysis and found that the period of oscillation became around four times shorter when the laser power increased from 10 to 37 mW, for example, as shown in Fig. 4a and Movies S3 and S4, respectively. On the other hand, the rotation amplitude did not significantly change (Fig. 4a). When we plotted the rotational frequencies of x and y, that we call f_x and f_y, respectively, against the laser power, we found that they followed linear trends. Indeed, when we fitted the data to straight lines, we obtained coefficients of determination $R^2 \geq 0.99$, Fig. 4b. As mentioned before and shown in Fig. 4b the rotational frequencies f_x and f_y were almost coincident, and so they were the values of the linear fitting parameters.

We then evaluated the power spectral density (PSD) of the rotation of a trapped FC-in-HC droplet, a quantity related to the trap stiffness. The typical shape of a PSD *vs.* frequency plot for a trapped particle shows an initial *plateu* at low frequencies indicating trapping, since the particle cannot move arbitrarily far from the trap. This plateau is followed by a decay at higher frequencies related to a behaviour similar to free diffusion. For a rotating droplet under a laser power of 10 mW we did not observe this type of shape (Fig. 5a and b), but a monotonic decrease of the PSD superimposed at low frequencies. Similarly to what was observed for the trajectories obtained from image analysis, the PSD data for both the x and y traces were almost coincident (Fig. 5a and b, respectively), and this was the case for all the laser powers. Noteworthily, when the laser power was raised, the shape of the PSD plot in the low frequency range (around 1–100 Hz) changed. Specifically, a visible peak at low frequencies appeared in the plots along with some harmonics at higher frequencies, as opposed to the continuous decrease observed at 10 mW (Fig. 5c). The appearance of such a peak at low frequencies is related to trapped particles experiencing some additional motion. In our case, the peak can be ascribed to the rotational motion of the droplets. Interestingly, the peak shifted to higher frequencies as the laser power increased, which could be related to the increase of the rotation frequency of the droplets. In fact, the frequency at which the main peak appeared for each power approximately coincided with the rotational frequency measured from the video tracking (Fig. 4b), demonstrating that the type of rotation described here can be directly inferred from the PSD.[28] Because the droplets did rotate at a laser power of 10 mW, as demonstrated in video recordings, the corresponding low-frequency peak in that case likely fell outside the lower limit of the frequency range. Fitting the PSD *vs.* frequency plots to eqn (1) (Fig. 5a and b) we were able to quantify the cutoff frequency, f_c, for all laser powers, which defines the limits to accurately determine the dynamics of the system. As seen in Fig. 5d, the cutoff frequency also increased with the laser power (roughly

 This journal is © The Royal Society of Chemistry 2025

Open Access Article. Published on 30 Juli 2025. Downloaded on 02.04.2026 06:31:57.
This article is licensed under a Creative Commons Attribution-NonCommercial 3.0 Unported Licence.

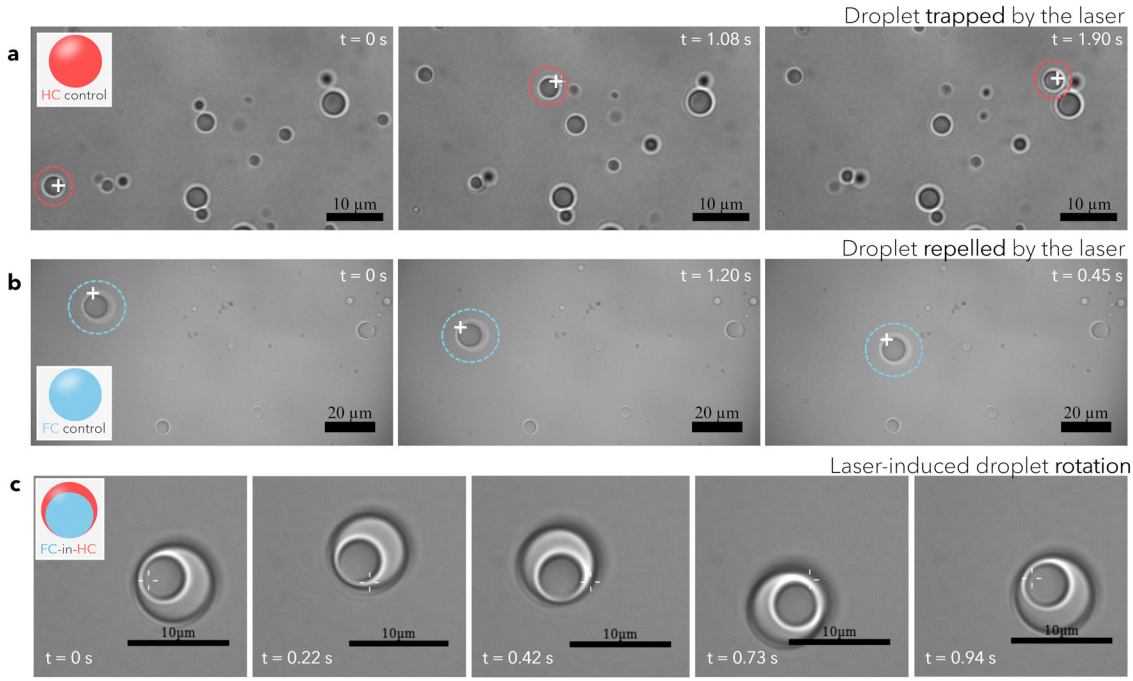

Fig. 2 Optical microscope snapshots of monophase droplets consisting of pure HC (a) and FC (b) oils as well as FC-in-HC droplets (c) in the optical tweezers chamber; an indication of the position of the beam is indicated with a cross symbol. HC oil droplets (refractive index higher than that of water) were successfully trapped and could be moved along with the beam (a). Conversely, FC oil droplets (refractive index lower than that of water) were repelled by the laser, pushing them away from it, which also resulted in net droplet translation (b). On the other hand, FC-in-HC droplets, with an asymmetric distribution of the refractive index, were successfully trapped and experienced an anomalous rotational motion around the axis of the beam of well-defined period (laser power 10 mW) (c).

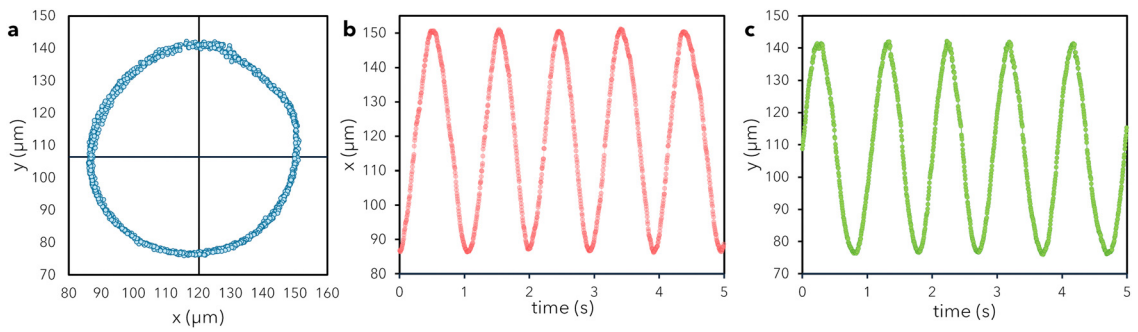

Fig. 3 (a) Trajectory plot (*i.e.*, *y vs. x* coordinate plot) of the middle point between the foci of the ellipse to which we fitted the contour of a FC-in-HC rotating droplet using a Python script (see Methods). The data confirm that the droplet experienced a rotational motion at 10 mW of laser power. (b) and (c) Temporal evolution of coordinates *x* (b) and *y* (c) for the same droplet. The two quantities described oscillatory motion characterized by regular amplitude and frequency. All plots correspond to the image analysis of the initial five seconds of droplet rotation.

following a linear tendency), showing similar values for fittings to the *x* and *y* traces and thus, consistent with the image analysis of the trajectories.

We emphasize that rotation is achieved with a laser beam that is linearly polarized, *i.e.*, not carrying any angular momentum. Such rotation with a linearly polarized beam has been explained in terms of the so-called windmill effect.[29–32] In this situation, the anisotropy of the trapped object is responsible for the deflection of the light rays as they pass through it, and the change in light momentum imparts a torque on the trapped object, initiating the rotation. This torque is counterbalanced by the drag force of the liquid, setting a constant rotation velocity in the steady state. From an experimental point of view, optically induced rotation with light not carrying any angular momentum has only been shown (to the best of our knowledge) in anisotropic micro-objects made with complicated microfabrication techniques (micromachining and two-photon polymerization),[32] and more recently in a triplet of colloidal beads.[33] In the latter, one of the beads was thermally active (*i.e.*, absorbing) and generated a temperature gradient which led to imbalanced thermophoretic forces and torques.[33] However, rotation of trapped liquid-based objects has not been

Open Access Article. Published on 30 Juli 2025. Downloaded on 02.04.2026 06:31:57.
This article is licensed under a Creative Commons Attribution-NonCommercial 3.0 Unported Licence.

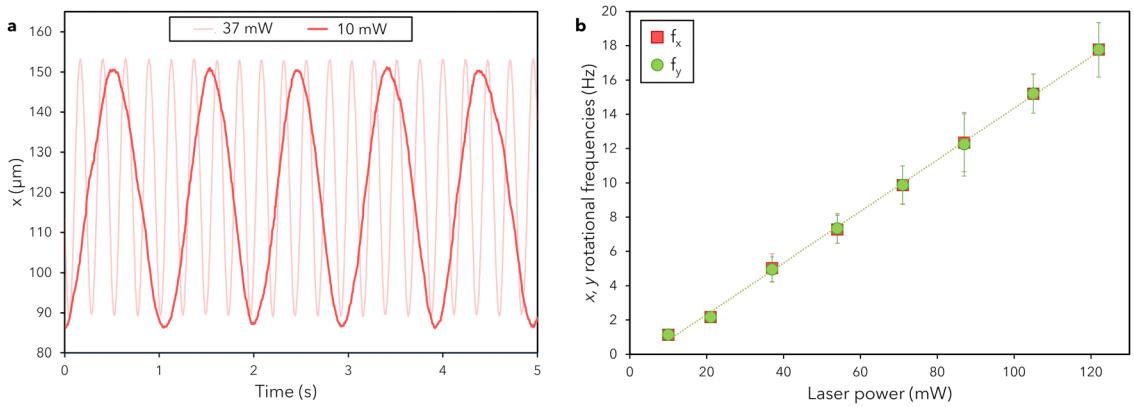

Fig. 4 (a) Plot of the temporal evolution of the x coordinate for a FC-in-HC droplet at two different laser powers: 10 and 37 mW. The rotation frequency at 37 mW was roughly four times higher than at 10 mW. (b) Plots of the rotation frequencies of x (squares) and y (circles) against the laser power (P) showing linear trends. Linear fitting equations and determination coefficients are: f_x (Hz) = $a + b{\cdot}P$(mW) with a = (−0.68 ± 0.15) Hz and b = (0.1504 ± 0.0020) Hz mW^{-1} (R^2 = 0.9989); f_y (Hz) = $c + d{\cdot}P$(mW) with c = (−0.69 ± 0.15) Hz and d = (0.1472 ± 0.0020) Hz mW^{-1} (R^2 = 0.9989). Each data point corresponds to the average frequency obtained by fitting graphs like that in (a) to a sine for 1, 2, 5, 10, 20 and 30 s, for three individual droplets; error bars correspond to standard deviations.

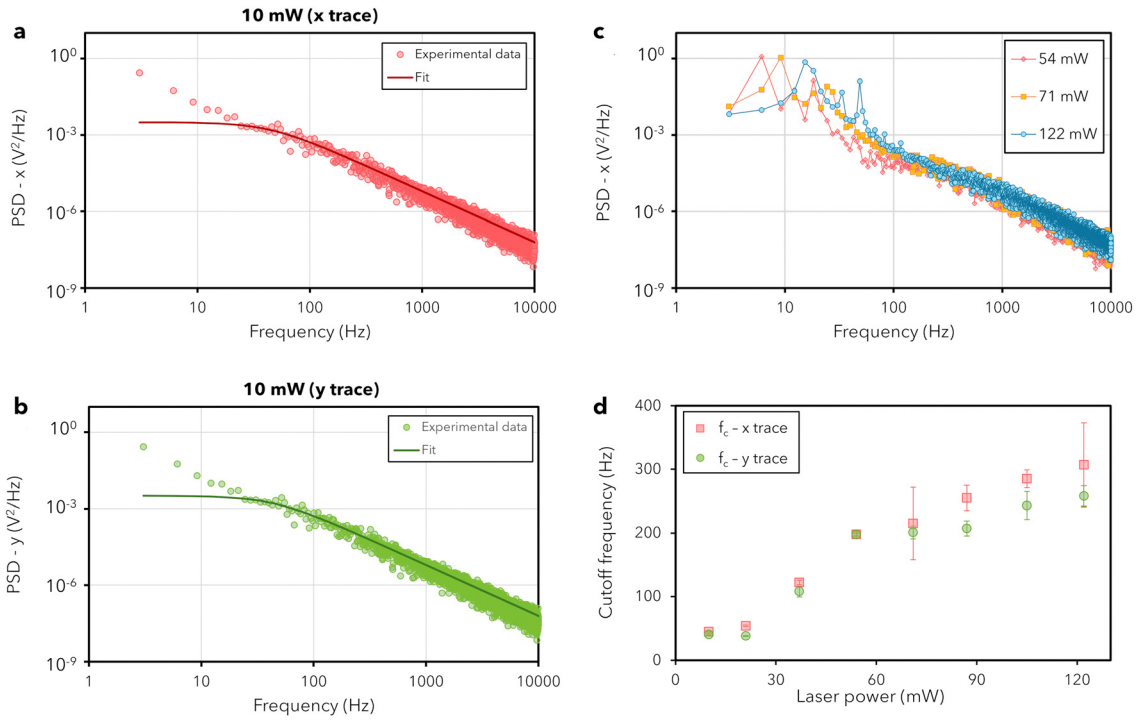

Fig. 5 (a) Plot of the x trace of the power spectral density (PSD) against the frequency for a FC-in-HC droplet rotating at a laser power of 10 mW. The PSD monotonically decreased with the frequency. Symbols and line correspond to experimental points and fit to eqn (1), respectively. (b) Same as (a) but for the y trace of the PSD. (c) PSD plots for three powers of the laser beam: 54 (diamonds), 71 (squares) and 122 (circles) mW. A main peak and corresponding harmonics can be seen in the low frequency part of the PSD. These peaks shifted to higher frequencies when the laser power was raised. (d) Cutoff frequency obtained from fits of the PSD plots (like those shown in (a) and (b)) to eqn (1). The cutoff frequency increased with the laser power and showed similar values for fittings to both the x (squares) and y (circles) traces.

demonstrated. The rotation of non-spherical objects like those of our design in optical trapping setups has been theoretically discussed in refs.[17,34] providing a brief explanation of a computation method to estimate the forces, which is out of the scope of the present work. As explained above, biphasic droplets with the opposite morphology, *i.e.*, HC-in-FC droplets did not rotate when the beam was switched on (see Movie S5). We hypothesize that this lack of rotation could be related to the opposite optical characteristics of these droplets compared to the FC-in-HC droplets. However, further work and theoretical modeling are needed to elucidate the mechanism behind droplet rotation.

 This journal is © The Royal Society of Chemistry 2025

Open Access Article. Published on 30 Juli 2025. Downloaded on 02.04.2026 06:31:57.
This article is licensed under a Creative Commons Attribution-NonCommercial 3.0 Unported Licence.

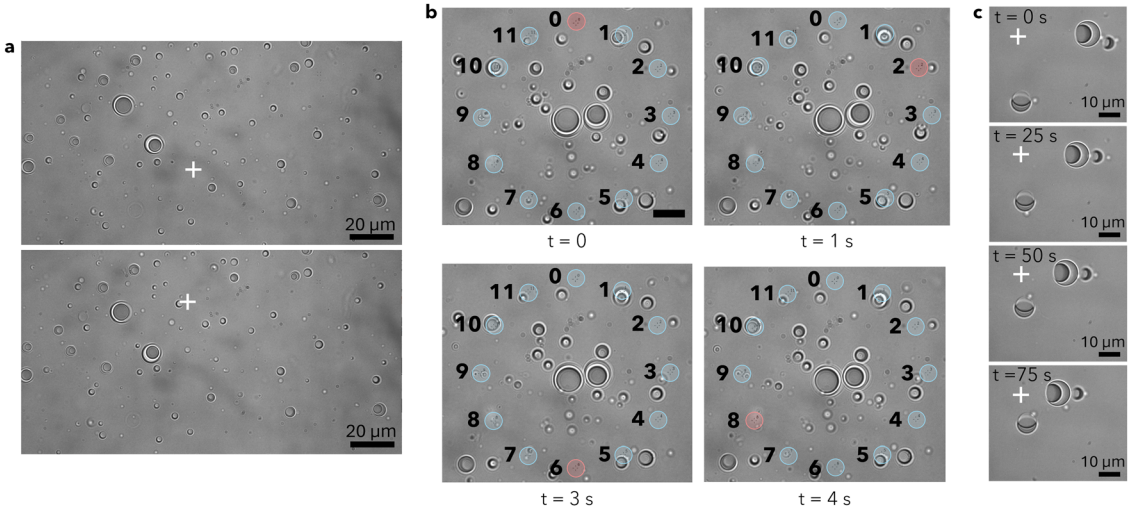

Fig. 6 (a) Optical microscope pictures (from Movie S6) showing FC-in-HC droplets tilted with the inner phase facing the laser beam (indicated with a cross symbol). (b) Optical microscope snapshots from Movie S7 where optical traps (highlighted by blue circles) are arranged into a circumference following a 12-hour clock. The droplets at the centre of the circumference rotate when the traps are sequentially activated (the activated trap is indicated with a red circle) to enable orientation of the inner phase towards the laser beam. (c) Optical microscope pictures (from Movie S10) showing the translation motion of two FC-in-HC droplets towards the laser beam (indicated with a cross symbol) at a speed of around 0.25 μm s^{-1}.

Even though HC-in-FC did not spontaneously rotate in the same out-of-equilibrium, dissipative, way as the FC-in-HC droplets when trapped, both HC-in-FC and FC-in-HC droplets could be externally rotated in a user-defined way if they were not trapped. Indeed, we had observed that when the laser beam was focused in the vicinity of the droplets (*i.e.*, not trying to trap them), both types of droplets tilted with the internal phase of the droplet facing the beam (see Fig. 6a and Movie S6). A similar tilt has been described by Nagelberg *et al.*[35] who attributed it to optothermally induced Marangoni flows. In particular, the thermal gradient induced by the laser beam leads to an interfacial tension differential across the inner interface (*i.e.*, HC oil-FC oil) of the biphase droplets, which is surfactant-free, causing internal Marangoni flows and a net torque.[35] Encouraged by this behaviour, we set up twelve traps arranged in a circumference, like the numbers on a 12-hour clock. When we activated them sequentially with a dwell time of 500 ms, FC-in-HC droplets placed near the centre of the circumference started to rotate following the beam, resembling the hands of the clock (see Fig. 6b and Movie S7). Decreasing the dwell time to 50 ms led to faster, rather continuous, rotation (Movie S8). HC-in-FC droplets could also be externally rotated in the same way (Movie S9). Tilting and motion towards a UV light beam of biphasic oil-in-water droplets were also recently demonstrated by Frank *et al.*[19] However, in their case, UV irradiation resulted in non-uniform trans-cis isomerization of the azobenzene-based hydrocarbon surfactant used in droplet formulation. The resulting gradient of hydrocarbon surfactant across the sample led to droplet motion (*i.e.*, Marangoni effect). We also observed FC-in-HC droplet translation when shining the laser in the droplet vicinity, of speed around 0.25 μm s^{-1} at a laser power of 20 mW (Fig. 6c and Movie S10). When many droplets were present, they translated and gathered around the laser beam roughly in a radial pattern (Fig. S4 and Movie S11), as previously described for iododecane-ethoxynonafluorobutane biphasic droplets shined with a 780 nm laser beam.[21] Although we hypothesize that droplet translation might be associated with optothermally induced Marangoni flows as well, future modelling work is needed to elucidate the mechanisms behind this behaviour.[36] Interestingly, FC-in-HC droplet translation occurs with the FC side facing the laser beam. Since the FC oil has a lower refractive index than water, repulsion occurs when the droplet is close to the laser focus, since the gradient optical force is negative due to the negative sign of the refractive index mismatch. Therefore, droplets stop their translation motion at a certain distance from the beam, where the two effects, namely optical repulsion and attraction to the beam due to Marangoni flows, are balanced, as shown in Movies S10 and S11.

Conclusions

In summary, we have demonstrated an anomalous, out-of-equilibrium, rotation of biphasic droplets trapped in an optical tweezers setup. These oil-in-water droplets consisted of a mixture of two immiscible oils at room temperature: a hydrocarbon (HC) oil and a fluorocarbon (FC) oil, with refractive indexes higher and lower than the refractive index of water, respectively. We attribute this behaviour to the change in momentum of light that occurs due to the asymmetric distribution of the refractive index within the droplets, that results in a torque applied to the droplet, though this mechanism might become more complicated by the presence of Marangoni flows generated by laser light absorption. Notably, only droplets in which the HC oil encapsulated the FC oil (FC-in-HC droplets) rotated with well-defined amplitude and period under the laser beam. The opposite

Open Access Article. Published on 30 Juli 2025. Downloaded on 02.04.2026 06:31:57.
This article is licensed under a Creative Commons Attribution-NonCommercial 3.0 Unported Licence.

morphology (HC-in-FC droplets) only displayed a slight vibrational motion. We hypothesize that this could be due to the different interaction with light of the two morphologies.

In addition to out-of-equilibrium rotation when the droplets were trapped, we have shown that droplets that do not interact directly with the trapping beam can also be rotated. This is achieved because when the beam was focused in their vicinity, both types of droplets, HC-in-FC and FC-in-HC, tilted with the inner phase facing the beam. Arranging multiple traps into a circumference and activating them sequentially led to rotation of the droplets. Altogether, our results demonstrate that both out-of-equilibrium and indirect rotation of biphasic droplets can be achieved in optical tweezers, which has implications not only from the fundamental point of view, but also in potential applications of the phenomenon, such as optically induced mixing, and related applications that are being developed in the emerging field of optofluidics.[37–40] Future work, including the quantification of the optical torque both from experiments and computer simulations, will further elucidate the mechanisms behind the observed phenomenology.

Author contributions

Jesús J. del Pozo (data curation: lead; formal analysis: lead; investigation: lead; methodology: lead; software: lead; visualization: lead; writing – review & editing: equal). Ana B. Bonhome-Espinosa (data curation: lead; formal analysis: lead; investigation: lead; methodology: lead; visualization: lead; writing – review & editing: equal). Wei Sun (data curation: equal; investigation: equal; methodology: equal; validation: equal; writing – review & editing: supporting). Carlos Gutiérrez-Ariza (formal analysis: equal; methodology: equal; software: equal). Raúl A. Rica-Alarcón (conceptualization: equal; data curation: equal; formal analysis: equal; funding acquisition: lead; methodology: lead; project administration: lead; resources: lead; supervision: lead; visualization: equal; writing – original draft: equal; writing – review & editing: equal). Laura Rodriguez Arco, PhD (conceptualization: lead; data curation: equal; formal analysis: equal; funding acquisition: lead; methodology: equal; project administration: lead; resources: lead; supervision: lead; visualization: lead; writing – original draft: lead; writing – review & editing: lead)

Conflicts of interest

There are no conflicts to declare.

Data availability

Data for this article, including trajectories, power spectral density data, and calculated frequencies are available at figshare at **https://doi.org/10.6084/m9.figshare.27908349.v1**.

SI Movies S1 to S11 (.mp4 format) and a PDF file with captions for SI Movies and Fig. S1–S4. See DOI: **https://doi.org/10.1039/d5sm00273g**

Acknowledgements

The authors acknowledge funding through grant P20_00340 funded by FEDER/Junta de Andalucía - Consejería de Transformación Económica, Industria, Conocimiento y Universidades. A. B. B.-E. also acknowledges co-founding by European Social Fund and Ministry of Economic Transformation, Industry, Knowledge and Universities of the Junta de Andalucía (PAIDI 2020). L. R.-A acknowledges fellowship Juan de la Cierva Incorporación IJC2018-037951-I funded by MCIN/AEI/10.13039/501100011033 and the University of Granada for funding her salary. W. S., C. A. G. and R. A. R. acknowledge financial support from Grant PID2021-127427NB-I00 funded by MICIU/AEI/10.13039/501100011033 and, by ''ERDF/EU''''. Funding for open access charge: Universidad de Granada.

References

1 A. deMello, Control and detection of chemical reactions in microfluidic systems, *Nature*, 2006, **442**, 394–402, DOI: **10.1038/nature05062**.
2 M. Zhang, A. E. Vokoun, B. Chen, W. Deng, R. L. Dupont, Y. Xu and X. Wang, Advancements in droplet reactor systems represent new opportunities in chemical reactor engineering: A perspective, *Can. J. Chem. Eng.*, 2023, **101**(9), 5189–5207, DOI: **10.1002/cjce.24897**.
3 T. Rossow, P. S. Lienemann and D. J. Mooney, Cell microencapsulation by droplet microfluidic templating, *Macromol. Chem. Phys.*, 2016, **218**(2), 1600380, DOI: **10.1002/macp.201600380**.
4 M. Sulliger, J. O. Arroyo and R. Quidant, *High throughput spectroscopy of pL droplets*, *arXiv*, 2024, *preprint*, DOI: **10.48550/arXiv.2403.04027**.
5 G. Cheng, C. Y. Kuan, K. W. Lou and Y.-P. Ho, Light-responsive materials in droplet manipulation for biochemical applications, *Adv. Mater.*, 2024, 2313935, DOI: **10.1002/adma.202313935**.
6 G. Villar, A. D. Graham and H. Bayley, A tissue-like printed material, *Science*, 2013, **340**, 48–52, DOI: **10.1126/science.1229495**.
7 G. Volpe, O. M. Maragò, H. Rubinsztein-Dunlop, G. Pesce, A. B. Stilgoe, G. Volpe and G. A. Swartzlander, Roadmap for optical tweezers, *J. Phys. Photonics*, 2023, **5**(2), 022501, DOI: **10.1088/2515-7647/acb57b**.
8 E. Ortiz-Rivero, C. D. González-Gómez, R. A. Rica and P. Haro-González, Effect of the photoexcitation wavelength and polarization on the generated heat by a Nd-doped microspinner at the microscale, *Small*, 2024, **20**, 2308534, DOI: **10.1002/smll.202308534**.
9 S. Li, C. Hu, X. Gao, G. Ma, H. Li, X. Hu and X. Hu, Optical tweezers assisted controllable formation and precise manipulation of microdroplet, *Appl. Phys. Express*, 2019, **12**, 117001, DOI: **10.7567/1882-0786/ab474f**.
10 M. Tanaka, Y. Tsuboi and K. Yuyama, Formation of a core–shell droplet in a thermo-responsive ionic liquid/water

 This journal is © The Royal Society of Chemistry 2025

Open Access Article. Published on 30 Juli 2025. Downloaded on 02.04.2026 06:31:57.
This article is licensed under a Creative Commons Attribution-NonCommercial 3.0 Unported Licence.

mixture by using optical tweezers, *Chem. Commun.*, 2022, **58**, 11787–11790, DOI: 10.1039/D2CC02699F.

11 A. Chen, S. W. Li, F. N. Sang, H. B. Zeng and J. H. Xu, Interactions between micro-scale oil droplets in aqueous surfactant solution determined using optical tweezers, *J. Colloid Interface Sci.*, 2018, **532**, 128–135, DOI: 10.1016/j.jcis.2018.07.116.

12 A. Chen, X. Liu, Y. We, G. Luo and J.-H. Xu, Interactions between CO2-responsive switchable emulsion droplets determined by using optical tweezers, *Langmuir*, 2020, **36**, 4600–4606, DOI: 10.1021/acs.langmuir.0c00203.

13 M. R. Griffiths, A. Raudsepp, K. M. McGrath and M. A. K. Williams, Measuring the interaction between a pair of emulsion droplets using dual-trap optical tweezers, *RSC Adv.*, 2016, **6**, 14538–14546, DOI: 10.1039/C5RA25073K.

14 S. Lach, S. M. Yoon and B. A. Grzybowski, Tactic, reactive, and functional droplets outside of equilibrium, *Chem. Soc. Rev.*, 2016, **45**, 4766–4796, DOI: 10.1039/c6cs00242k.

15 D. Lohse and X. Zhang, Physicochemical hydrodynamics of droplets out of equilibrium, *Nat. Rev. Phys.*, 2020, **2**, 426–443, DOI: 10.1038/s42254-020-0199-z.

16 A. Ashkin, Optical trapping and manipulation of neutral particles using lasers, *Proc. Natl. Acad. Sci. U. S. A.*, 1997, **94**, 4853–4860, DOI: 10.1073/pnas.94.10.4853.

17 G. Pesce, P. H. Jones, O. M. Maragò and G. Volpe, Optical tweezers: theory and practice, *Eur. Phys. J. Plus*, 2020, **135**, 949, DOI: 10.1140/epjp/s13360-020-00843-5.

18 S. E. S. Spesyvtseva and K. Dholakia, Trapping in a material world, *ACS Photonics*, 2016, **3**, 719–736, DOI: 10.1021/acsphotonics.6b00023.

19 L. D. Zarzar, V. Sresht, E. M. Sletten, J. A. Kalow, D. Blankschtein and T. M. Swager, Dynamically reconfigurable complex emulsions via tunable interfacial tensions, *Nature*, 2015, **518**, 520–524, DOI: 10.1038/nature14168.

20 B. D. Frank, S. Djalali, A. W. Baryzewska, P. Giusto, P. H. Seeberger and L. Zeininger, Reversible morphology-resolved chemotactic actuation and motion of Janus emulsion droplets, *Nat. Commun.*, 2022, **13**, 2562, DOI: 10.1038/s41467-022-30229-3.

21 C. H. Meredith, A. C. Castonguay, Y.-J. Chiu, A. M. Brooks, P. G. Moerman, P. Torab, P. K. Wong, A. Sen, D. Velegol and L. D. Zarzar, Chemical design of self-propelled Janus droplets, *Matter*, 2022, **5**, 616–633, DOI: 10.1016/j.matt.2021.12.014.

22 L. D. Zarzar, J. A. Kalow and X. He, *et al.*, Optical visualization and quantification of enzyme activity using dynamic droplet lenses, *Proc. Natl. Acad. Sci. U. S. A.*, 2017, **114**, 3821–3825, DOI: 10.1073/pnas.1618807114.

23 S. Nagelberg, L. D. Zarzar, N. Nicolas, K. Subramanian, J. A. Kalow, V. Sresht, D. Blankschtein, G. Barbastathis, M. Kreysing, T. M. Swager and M. Kolle, Reconfigurable and responsive droplet-based compound micro-lenses, *Nat. Commun.*, 2017, **8**, 14673, DOI: 10.1038/ncomms14673.

24 S. Nagelberg, A. Goodling, B. Kaehr, M. Kolle and L. Zarzar, Structural color due to interference of totally internally reflected light in bi-phase droplets, *Imag. Appl. Optics*, 2019, paper IM2B.4, DOI: 10.1364/ISA.2019.IM2B.4.

25 S. K. Y. Tang, Z. Li, A. R. Abate, J. J. Agresti, D. A. Weitz, D. Psaltis and G. M. Whitesides, A multi-color fast-switching microfluidic droplet dye laser, *Lab Chip*, 2009, **9**, 2767–2771, DOI: 10.1039/b908593g.

26 D. Bronte Ciriza, A. Callegari, M. G. Donato, B. Çiçek, A. Magazzù, I. Kasianiuk and O. M. Maragò, Optically driven Janus microengine with full orbital motion control, *ACS Photonics*, 2023, **10**, 3223–3232, DOI: 10.1021/acsphotonics.3c00630.

27 V. M. Babović and S. Mekić, The Bravais pendulum: the distinct charm of an almost forgotten experiment, *Eur. J. Phys.*, 2011, **32**, 1077, DOI: 10.1088/0143-0807/32/4/020.

28 B. Roy, S. K. Bera and A. Banerjee, Simultaneous detection of rotational and translational motion in optical tweezers by measurement of backscattered intensity, *Opt. Lett.*, 2014, **39**, 3316–3319, DOI: 10.1364/OL.39.003316.

29 E. Higurashi, O. Ohguchi, T. Tamamura, H. Ukita and R. Sawada, Optically induced rotation of dissymmetrically shaped fluorinated polyimide micro-objects in optical traps, *J. Appl. Phys.*, 1997, **82**, 2773–2779, DOI: 10.1063/1.366163.

30 P. Galajda and P. Ormos, Complex micromachines produced and driven by light, *Appl. Phys. Lett.*, 2001, **78**, 249–251, DOI: 10.1063/1.1339258.

31 P. Galajda and P. Ormos, Rotors produced and driven in laser tweezers with reversed direction of rotation, *Appl. Phys. Lett.*, 2002, **80**, 4653–4655, DOI: 10.1063/1.1480885.

32 E. Higurashi, H. Ukita, H. Tanaka and O. Ohguchi, Optically induced rotation of anisotropic micro-objects fabricated by surface micromachining, *Appl. Phys. Lett.*, 1994, **64**, 2209–2210, DOI: 10.1063/1.111675.

33 R. Chand, C. E. Rani, D. Paul and G. V. P. Kumar, Emergence of directional rotation in an optothermally activated colloidal system, *ACS Photonics*, 2023, **10**, 4006–4013, DOI: 10.1021/acsphotonics.3c00890.

34 P. Jones, O. Maragó and G. Volpe, *Optical tweezers*, 2015, Cambridge University Press, Cambridge.

35 S. Nagelberg, J. F. Totz, M. Mittasch, V. Sresht, L. Zeininger, T. M. Swager, M. Kreysing and M. Kolle, Actuation of Janus Emulsion Droplets via Optothermally Induced Marangoni Forces, *Phys. Rev. Lett.*, 2021, **127**, 144503, DOI: 10.1103/PhysRevLett.127.144503.

36 K. Dietrich, N. Jaensson, I. Buttinoni, G. Volpe and L. Isa, Microscale Marangoni surfers, *Phys. Rev. Lett.*, 2020, **125**, 098001, DOI: 10.1103/PhysRevLett.125.098001.

37 S. Mandal and D. Erickson, in Optofluidics – Applications. ed. D. Li, *Encyclopedia of microfluidics and nanofluidics*, Springer, Boston, MA, 2008, DOI: 10.1007/978-0-387-48998-8_1163.

38 M. Fränzl and F. Cichos, Hydrodynamic manipulation of nano-objects by optically induced thermo-osmotic flows, *Nat. Commun.*, 2022, **13**, 656, DOI: 10.1038/s41467-022-28212-z.

39 J. S. Donner, G. Baffou, D. McCloskey and R. Quidant, Plasmon-assisted optofluidics, *ACS Nano*, 2011, **5**(7), 5457–5462, DOI: 10.1021/nn200590u.

40 D. Hess, T. Yang and S. Stavrakis, Droplet-based optofluidic systems for measuring enzyme kinetics, *Anal. Bioanal. Chem.*, 2020, **412**, 3265–3283, DOI: 10.1007/s00216-019-02294-z.